

# “Albedo dome”: a method for measuring spectral flux-reflectance in a laboratory for media with long optical paths

BONNIE LIGHT,<sup>1,2,\*</sup> REGINA C. CARNES,<sup>3</sup> AND STEPHEN G. WARREN<sup>2,3</sup>

<sup>1</sup>Polar Science Center, Applied Physics Laboratory, University of Washington, Seattle, Washington 98105, USA

<sup>2</sup>Department of Atmospheric Sciences, University of Washington, Seattle, Washington 98195, USA

<sup>3</sup>Department of Earth and Space Sciences, University of Washington, Seattle, Washington 98195, USA

\*Corresponding author: [bonnie@apl.washington.edu](mailto:bonnie@apl.washington.edu)

Received 7 January 2015; revised 23 April 2015; accepted 24 April 2015; posted 4 May 2015 (Doc. ID 232083); published 2 June 2015

A method is presented for accurate measurement of spectral flux-reflectance (albedo) in a laboratory, for media with long optical path lengths, such as snow and ice. The approach uses an acrylic hemispheric dome, which, when placed over the surface being studied, serves two functions: (i) it creates an overcast “sky” to illuminate the target surface from all directions within a hemisphere, and (ii) serves as a platform for measuring incident and backscattered spectral radiances, which can be integrated to obtain fluxes. The fluxes are relative measurements and because their ratio is used to determine flux-reflectance, no absolute radiometric calibrations are required. The dome and surface must meet minimum size requirements based on the scattering properties of the surface. This technique is suited for media with long photon path lengths since the backscattered illumination is collected over a large enough area to include photons that reemerge from the domain far from their point of entry because of multiple scattering and small absorption. Comparison between field and laboratory albedo of a portable test surface demonstrates the viability of this method. © 2015 Optical Society of America

**OCIS codes:** (120.0120) Instrumentation, measurement, and metrology; (280.0280) Remote sensing and sensors; (120.3150) Integrating spheres; (120.5630) Radiometry; (120.5820) Scattering measurements; (160.4760) Optical properties.

<http://dx.doi.org/10.1364/AO.54.005260>

## 1. INTRODUCTION

The flux-reflectance, or “albedo,” is the fraction of incident solar radiation backscattered by a planetary surface, cloud, or the Earth–atmosphere system. The surface albedo is a major determinant of the surface heat budget. Quantitative information about the surface heat budget is essential for an understanding of climate. Regions of the planet with high surface albedo (e.g., snow, ice) respond differently to solar heating than regions with low surface albedo (e.g., water, wet soil, tundra, forest). Such contrasts in surface albedo can lead to climatically sensitive feedback. One example of this contrast occurs in the polar oceans, where the open ocean has broadband (visible and near-infrared) albedo of typically less than 0.1 [1] and the frozen sea surface has broadband albedo of typically 0.4–0.9, depending on the state of the ice surface [2]. This contrast drives a positive feedback [3,4] capable of amplifying ice retreat or expansion. Our present understanding of Earth’s climate indicates that this sensitive positive feedback has been contributing to the anomalously large temperature increases seen at high latitudes in response to increased greenhouse gases in Earth’s atmosphere [5–8]. While gross features of Earth’s

climate can be understood with knowledge of the spatially averaged planetary albedo, the most informative climate models require detailed information about the spatial and temporal distribution of albedo of different surface types and states.

Ground-based measurement of surface albedo in a field setting is typically straightforward (for example, see work by Levinson *et al.* [9]). If a relatively small area (approximately 12 m<sup>2</sup>) of the surface can be considered representative, and the measurement site is accessible during sunlit hours, then albedo measurement requires little more than a single radiometer outfitted with an appropriate cosine collector (for example, see Grenfell *et al.* [10]). The radiometer is turned upward to measure the downwelling irradiance (flux), then turned downward to measure the backscattered irradiance. The ratio of the two irradiances is the albedo for that surface type. Measurements of homogeneous and planar surfaces are the most generally applicable. The plane of the radiometer should be parallel to the surface. If the surface is horizontal, a leveling device on the radiometer ensures that the respective fields of view capture only the surface and only the sky. Spectral data provide the most broadly applicable estimates; broadband

measurements are inherently dependent on the spectral distribution of incident radiation. Measurements made under cloud cover, where incident light is notably more diffuse, are most accurate, because errors caused by surface slope and tilt of the radiometer are then minimized. Measurements made while the ambient illumination is constant over the measurement interval provide the highest quality data. If the radiometer and accompanying support are properly configured, then the need for shadowing corrections is minimized to typically a few percent. Figure 1 shows a “field” albedo being measured over the test surface used in this study. In this example, approximately 90% of the backscattered irradiance originates from within a 2 m radius, centered directly beneath the radiometer. For the purpose of building predictive tools, the most useful measurements are made over uniform surface type under either complete overcast skies or beneath clear skies with documented sun angle.

While measurements of naturally occurring surfaces under naturally occurring illumination are essential, there is also need for techniques to make albedo measurements in the laboratory. The ability to study surfaces that can be controlled, manipulated, or altered is necessary when such surfaces form only under unique conditions, are inaccessible in the field, or are useful proxies for past or future climates. Techniques for making laboratory albedo measurements exist, but they generally require more specialized corrections than their field albedo counterparts. Finite surface extent, artificial illumination, multiple light reflections in a confined space, instrument shadows on the surface, and unnatural variations in the angular

distribution of the incident illumination can be difficult to characterize and control in the laboratory. Since field albedo measurements are relatively simple, experiments carried out in the laboratory sometimes extend that simplicity indoors, in which a radiometer is used over the surface to look up and look down, and the resulting ratio is assumed to be an accurate estimate of the field albedo (for example, see Perovich and Grenfell [11]). Such measurements ignore the possibility of the instrumentation shadowing the surface, and there may be no attempt to characterize the geometry of the incident light field. More sophisticated techniques have been employed, where an integrating sphere is used to measure the albedo of a small sample volume [12]. In this case, however, only small samples were measured and it was necessary to ensure that the snow samples were densely packed to maximize the optical depth and reduce the distance that radiation traveled in the sample holder. To overcome this, corrections were necessary for extending this finite sample size measurement to a measurement appropriate for snow of infinite depth.

In some instances, where laboratory characterization of the apparent optical properties of a material are needed, the albedo is not quantified directly, but instead the angular reflectance [13–15] or bidirectional-reflectance distributions (BRDF) [16–20] are measured. While such measurements may contain considerably more information about the optical response of a surface than a simple albedo, and albedos may be calculated from these reflectance measurements, they also require more complex instrumentation and a more complicated measurement protocol. Furthermore, calculation of albedo from a BRDF measurement requires measurement of a standard of known BRDF, and is limited to opaque surfaces and the albedo resulting from direct illumination. While these various techniques have merits, we desired a technique that would be useful for characterizing the spectral albedo of laboratory-grown sea ice under a variety of conditions, temperatures, and histories, and where the need for corrections is minimized and the illuminated area and viewing area are large enough to directly capture the effects of multiple scattering radiative transport. In particular, media with long optical paths require samples and viewing geometries large enough to include photons that travel significant horizontal distances within the domain before reemerging to contribute to the backscattered light field. If the domain is small, then transport of such photons may be interrupted by the boundaries. If the viewing area is small, then photons that emerge far from their entry point will not be sampled. This paper describes an approach for making spectral albedo measurements on media with long optical paths, grown and maintained in a laboratory setting.

## 2. MOTIVATION FOR ALBEDO STUDIES OF LABORATORY-GROWN SEA ICE

If the albedo of a specific surface type on Earth is needed, the best approach is to travel to that surface and measure it directly. However, surfaces in remote regions may be inaccessible and some surfaces hypothesized to be prevalent in Earth’s past history or in the future may not exist naturally on modern Earth. Surrogates formed in the laboratory may be the only practical way to study such surfaces.



(a)



(b)

**Fig. 1.** (a) Photograph of measurement of “field albedo” for the white tarp test surface on a parking lot under overcast sky and schematic of apparatus used to make the albedo measurement. The end of the arm is equipped with a fiber optic cable that views a flat diffusely reflecting plate. The cable is coupled to a spectroradiometer. The apparatus in the schematic (b) is shown viewing the upward propagating backscattered light field. The arm would then be rotated to measure the downwelling incident light field. Photograph by B. Light.

One such surface that has gained attention in our laboratory is low-temperature sea ice. Paleoclimate records suggest periods in Earth's history known as "Snowball Earth" events, when surface temperatures and moisture budgets would likely have promoted the existence of bare, snow-free sea ice with temperature below  $-23^{\circ}\text{C}$  on the tropical oceans [21–23]. Ice such as this is not seen on modern Earth, where the frozen sea surface is typically covered by a layer of snow, which acts both to insulate the surface thermally, such that the ice rarely becomes colder than  $-23^{\circ}\text{C}$ , and conceal it optically, so that the optical properties of the ice itself rarely govern the surface albedo.

A distinguishing feature of ice grown on the ocean is the incorporation of numerous inclusions of liquid seawater throughout the ice matrix. For sea ice at moderate temperatures, these inclusions remain at least partially liquid, but as the ice is cooled, dissolved salts begin to precipitate [24]. In particular, as the temperature drops below  $-23^{\circ}\text{C}$ , crystals of sodium chloride dihydrate (hydrohalite) begin to crystallize. Light scattering from these crystals dramatically increases the surface albedo of cold sea ice. While this surface type is presently rare in nature [25], it is easily grown in the laboratory. Sublimation of this cold sea ice at consistently low temperatures would (after several years) result in a surface crust of hydrohalite salt formed as a lag deposit. Such a crust does not exist on sea ice anywhere on modern Earth, so it can be studied only in the laboratory. Speculation that the albedo of this surface type could be important for understanding the climate dynamics of Snowball Earth has motivated the development of a technique for reliably measuring the albedo of proxy surfaces grown and maintained in a walk-in freezer laboratory and not accessible using traditional field techniques.

### 3. APPROACH FOR LABORATORY ALBEDO MEASUREMENT

The design of this tool for laboratory albedo measurement was inspired by the concept of an integrating sphere, or in this case, half-sphere. The hemisphere, or "albedo dome," is large enough to fit over the surface of our laboratory ice tank ( $1.22\text{ m} \times 1.12\text{ m}$  in horizontal extent) and serves two essential functions: (i) the interior of the dome serves as a reflecting surface for providing diffuse downwelling illumination of the ice surface, and (ii) the dome itself serves as a platform for making measurements to estimate both downwelling irradiance incident on the surface and the upwelling irradiance backscattered by the surface. Figure 2 shows a schematic of the basic elements of the dome. The radius ( $R$ ) of the dome is 61 cm, the location of the reflecting plate is at the dome origin ( $R = 0$ ), and the location of the footprint on the surface is at  $R/2$ . A chimney for light entry was cut in the top of the dome. A collimated light source mounted exterior to the dome is directed into the dome, through the chimney, and onto a diffusely reflecting plate positioned on the ice surface. Light reflected from the plate illuminates the diffusely reflecting dome interior, which in turn illuminates the entire ice surface in the tank. The incident illumination reaching the surface is designed to simulate an idealized overcast sky. Estimates of the incident and backscattered light fields at the surface are made using a single fiber optic probe coupled to a spectroradiometer by viewing the

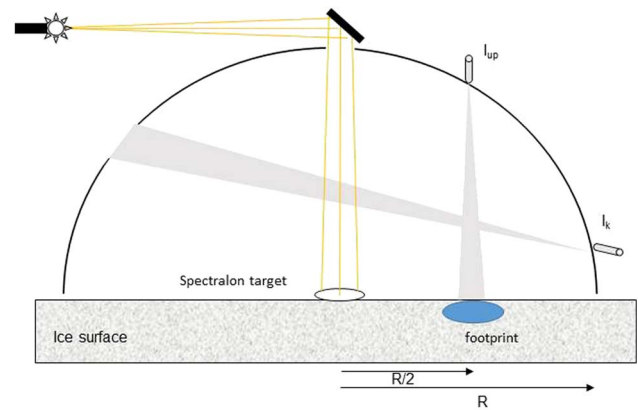


**Fig. 2.** Schematic of albedo dome over target surface. The dome has radius  $R$ . The center of the measurement footprint is positioned at  $R/2$ . The illumination source is indicated with yellow lines. Wedges indicate approximate fields of view, for example, measurement of incident radiance profile ( $I_k$ ) and backscattered radiance profile at  $0\text{ deg}$  ( $I_{up}$ ).  $I_k$  and  $I_{up}$  are measured with the fiber optic probe positioned in the viewing ports on the dome. The height of the  $I_{up}$  port is  $\frac{\sqrt{3}}{2}R$  above the ice surface. The dome used in this prototype has  $R = 61\text{ cm}$ .

dome interior wall and the target surface through port holes in the dome. The target surface is assumed to be approximately uniform, but the albedo of only a small area, or "footprint," is actually measured. Details of each component of the design follow.

#### A. Physical Layout

The maximum physical extent of the target surface and the albedo dome are limited only by space and cost. The minimum physical extent of the target surface and size of the dome are limited by the optical properties of the surface being measured. Media with relatively short optical path length can be measured with a relatively small dome. Media with longer optical path lengths require a larger dome for accurate measurement. If the finite extent of the dome affects the albedo at the footprint due to light leakage, either photons entering the study surface from outside the dome or photons escaping the study surface without detection, then the dome is not large enough. For example, in a weakly absorbing medium such as snow or ice at visible wavelengths, some of the light entering the surface from above will travel horizontally to the wall and be absorbed there, resulting in a low bias to the albedo estimate at wavelengths where the albedo is high. The minimum size of the tank holding the target surface requires that the measurement footprint be sufficiently far from tank edges to minimize the measurement of photons that have interacted with the walls of the enclosure. Such an effect would be difficult to correct for in this approach.

In the case of our cold sea ice, it was desired to measure the albedo evolution for ice growth and demise, so surface types with a wide variety of optical path lengths were studied. We thus chose to create a surface and use a dome as large as practical. The horizontal dimensions of the tank used for growing the ice were  $1.22\text{ m} \times 1.12\text{ m}$  (height  $1.24\text{ m}$ ; [www.bonarplastics.com/Products/BagintheBox.aspx](http://www.bonarplastics.com/Products/BagintheBox.aspx)). We used

an acrylic prefabricated dome with 1.22 m diameter (<http://plastic-domes-spheres.com/plastic-domes/>).

An acrylic dome was chosen because it was commercially available, lightweight, rigid, and capable of being painted. As purchased, the dome was transparent so it was necessary to prepare both the interior and exterior surfaces. To maximize the spectral reflectivity of the interior surface, it was painted with six coats of white latex paint followed by eight coats of white latex paint mixed with barium sulfate powder. When suspended in paint, barium sulfate is known to have diffuse reflectivity [26]. Tests were carried out to determine the maximum concentration of barium sulfate that left the paint still applicable (not too clumped) and with adequate bonding properties. A mass concentration of 30% barium sulfate was used. The goal for the surface preparation was to ensure that reflections off the dome interior would be as isotropic as possible with as high reflectivity as possible across the visible and near-infrared spectrum (wavelengths 350–2500 nm).

The exterior surface was treated to prevent leakage of ambient room light through the walls of the dome. To accomplish this, a single layer of black landscaping plastic was affixed to the exterior of the dome. Insulation was applied on top of the black plastic to prevent the plastic from overheating, as it was proximal to the light source, which occasionally became hot ( $>60^{\circ}\text{C}$ ) when in use, even within the freezer laboratory.

Figure 3 shows a photograph of the dome positioned on top of the tank. Locations on the dome (both interior and exterior) are referenced using latitude (specified by elevation angle,  $\theta$ ) and longitude (specified by azimuthal angle,  $\phi$ ). Three viewing ports were cut in the dome for access by the fiber optic probe. The longitude corresponding to the line of viewing ports is arbitrarily assigned  $\phi = 0$  and the three ports are at  $\theta = 60$ ,  $34.4$ , and  $10.3$  deg, corresponding to zenith viewing angles of  $0$ ,  $30$ , and  $70$  deg relative to the footprint. Each port opening was about 1 cm in diameter and the  $\theta = 60^{\circ}$  and  $34.4^{\circ}$  ports were equipped with fiber holders with fixed viewing angle. The  $\theta = 10.3^{\circ}$  port was left open so that the fiber could scan through the full range of angles to view the entire wall profile on the opposite side of the dome interior.

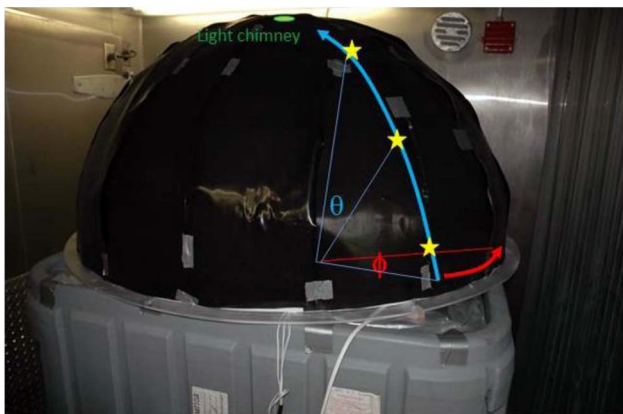


**Fig. 3.** Dome, mounted inside the freezer laboratory. Annotations show latitude ( $\theta$ ) and longitude ( $\phi$ ) reference frame and locations of viewing ports (yellow stars). The lights seen in this photograph are the room lights, which would normally be turned off during measurement. The experimental light source is not shown in this image.

## B. Surface Illumination

The albedo dome was designed to illuminate the study surface with diffuse light. We first attempted to accomplish this by mounting a point light source at the origin of the dome, but we were not successful at producing isotropic illumination. Furthermore, the source generated excessive heat inside the dome, which warmed the ice surface too much. A redesign of the apparatus moved the lamp outside of the dome. A tungsten–halogen bulb was positioned in a collimator (Oriol 66013 Lamp Housing with  $F/0.7$  fused silica condenser), and the collimated beam output was aimed at a mirror with broad spectral reflectivity (50-mm-diameter 1/10 wave mirror with UV enhanced aluminum coating, Edmund Optics part no. NT68-319) positioned on top of the dome. The mirror was set at a  $45$  deg angle; it reflected the horizontal beam downward through a 2 cm diameter entrance port cut in the top of the dome. The addition of a mirror in the optical path was necessary because of space limitations between the top of the dome and the ceiling of the cold room (approximately 10 cm). Due to this constraint, it was not possible to mount a light source with high intensity immediately above the dome. The light-entry port was fitted with a 10 cm long pipe to baffle the interior of the dome from stray light emanating directly from the lamp and grazing the port. The downwelling beam was aimed directly at a reflecting plate (20 cm in diameter) constructed from 6.35 mm thick Spectralon material (Labsphere, Inc.), which has approximate Lambertian reflectance. The plate rested on a small aluminum frame positioned on the measurement surface directly beneath the entrance port. Light reflected from the plate then illuminated the entire dome interior. As in an integrating sphere, multiple reflections between the high-reflectivity interior dome surface and the measurement surface enhanced the diffuseness of the light field on the dome walls.

A 750 W tungsten–halogen bulb with broad spectral output was chosen for the source. Since an albedo measurement is made at each wavelength, and since this technique makes use only of relative measurements, there was no need to simulate the spectral composition of natural sunlight. The spectroradiometer used for this study (FieldSpec Pro, manufactured by Analytical Spectral Devices) has sensitivity between 350 and 2500 nm wavelength, so there was no advantage in supplying illumination outside this wavelength range.

## C. Estimation of Downwelling Irradiance

The downwelling irradiance ( $F^{\downarrow}$ ) at the ice surface was estimated by integrating measurements of the wall-leaving radiance field [ $I(\theta, \phi)$ ] on the dome interior. To compute  $F^{\downarrow}$ , values of [ $I(\theta, \phi)$ ] are weighted by the cosine of their respective elevation angles and integrated over their respective solid angles:

$$F^{\downarrow} = \int_0^{2\pi} \int_0^{\pi/2} I(\theta, \phi) \cos \theta \sin \theta d\theta d\phi. \quad (1)$$

While the light leaving the dome wall was consistently diffuse, it was never isotropic. The radiance leaving any one point was assumed to be the same in all viewing directions, but radiances leaving the upper parts of the dome were generally larger than radiances leaving the lower parts. While  $I(\theta, \phi)$  was known to vary in  $\theta$ , it was assumed to be invariant in  $\phi$ . As a result, it was desired to measure the radiance profile with as much resolution

in  $\theta$  as practical. All  $I(\theta)$  were measured with the probe positioned just inside the 10.3 deg viewing port. A positioning guide was constructed from a piece of rigid acrylic to ensure that the hand-held fiber cable could be reliably repositioned at each viewing angle. Radiances were recorded at approximately 10 deg increments in  $\theta$ , with the probe aimed at positions on the dome interior corresponding to  $\theta = 0$  to 90 along  $\phi = 180$  deg (directly opposite the port longitude). For the convenience of summing discrete measurements, the  $I(\theta)$  are denoted  $I_k$  (where  $k = 0$  to 9 and  $\theta = 10k$  deg). Two examples of measured  $I_k$  profiles are shown in Fig. 4. The profile with larger raw instrument counts was measured above a fully developed hydrohalite crust with strong multiple scattering. The profile with lower counts was measured over a dissolving, wetted crust with weaker scattering. Clearly, the magnitude, and to some degree the shape, of these profiles depends on the character of the measurement surface. In fact, if the surface were black (completely absorbing), the only radiance reaching the dome walls would come directly from the Lambertian reflecting plate and there would be no multiple reflections within the dome. When viewed from any direction, the radiance leaving the plate should be isotropic. The intensity observed on the interior surface of the dome would not be uniform, but would vary as  $\sin\theta$ . Figure 4 includes this curve, although, since it was never measured, it is of arbitrary magnitude, and should be used only for comparing its shape with the other curves. If the measurement surface were also Lambertian, the radiance profile on the dome wall would be uniform, as would be found in a full integrating sphere.

Typically, measurements of the wall-leaving radiance were made only at  $k = 9, 8, 7, 6, 5, 4$ , and 3. Measurements at  $k = 2, 1$ , and 0 were impossible to make accurately because the reflecting plate either partially or fully obscured the field of view at these positions, contaminating the radiance measurement with directly reflected light. A linear extrapolation from the  $k = 3, 4$ , and 5 measurements was used to estimate  $I_k$  for  $k = 2, 1$ , and 0.

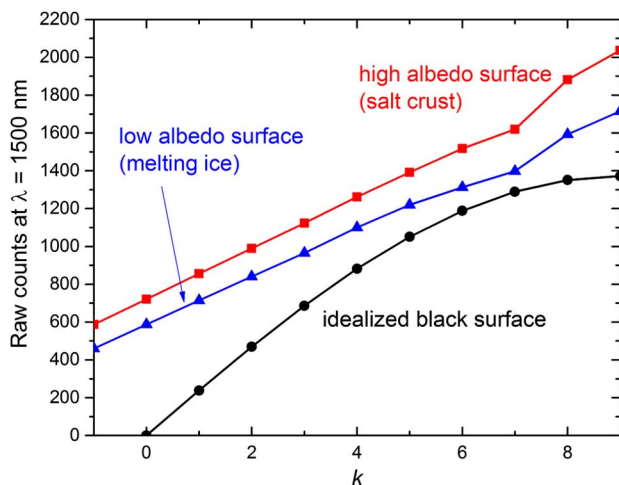


**Fig. 4.** Sample of typical downward radiance profiles incident on the more strongly scattering high albedo surface of a salt crust on ice and the lesser scattering surface of a low albedo melting ice surface.

Equation (1) gives the downwelling irradiance at the dome origin ( $R = 0$ ), and can be approximated as a sum over the individual contributions from a discrete set of measured radiances,  $I_k$ . For this experimental setup, however, it is necessary to compute the downwelling irradiance at the location of the footprint ( $R/2$ ), not  $R = 0$ . A coordinate transformation was thus necessary for assigning an appropriate weight for each measured radiance in the sum. Figure 5 illustrates the transformation, where the green hemisphere indicates the albedo dome on top of the ice surface. Green lines indicate constant  $\theta$  and constant  $\phi$ . The red interior dome represents a virtual hemisphere of arbitrary size centered on the target footprint ( $R/2, \phi = 0$ ). Red lines on the virtual dome indicate lines of constant elevation ( $\theta_f$ ) for all azimuth angles ( $\phi_f$ ) as referenced to the transformed coordinate system of the footprint. Red X's indicate  $k = 0$  to 9 positions where the radiance [ $I(\theta)$ ] is sampled on the dome wall and blue symbols show latitudinal bands from the virtual footprint hemisphere (constant  $\theta_f$ ) projected onto the albedo dome. The integration of downwelling irradiance at the footprint location ( $F_f^\downarrow$ ) is carried out by summing the radiance penetrating through each red band of constant  $\theta_f$  onto the footprint location. Equation (1), as applied to the target footprint, can be expressed as a sum of the discrete measurements  $I_k$ , weighted by coefficients  $C_k$ :

$$F_f^\downarrow = \sum_k C_k I_k. \quad (2)$$

The derivation of the  $C_k$  values is documented in Appendix A. For a footprint located at  $R/2$  and the height of the ice surface aligned with the base of the dome, the values of  $C_k$  ( $z = 0$ ) are given in the first row of Table 1 ( $z = 0$ ). Equation (2) is computed using raw spectroradiometer counts for  $I_k$  values, a convenience made possible by the fact that this albedo is a ratio of two radiometric quantities measured with

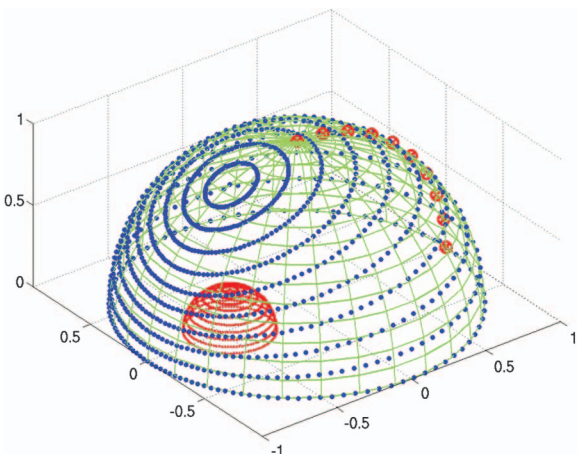


**Fig. 5.** Illustration showing geometry of coordinate transformation for calculation of downwelling incident irradiance at the location of the footprint (center of small red dome). Green mesh indicates lines of constant  $\theta, \phi$  on the albedo dome, the red dome is a virtual dome centered on footprint, with lines of constant  $\theta_f$ , red X's indicate locations where dome-leaving radiance is measured on the dome interior, and blue circles are red circles projected on to the albedo dome.

**Table 1. Weighting Coefficients ( $C_k$ ) for the Computation of Downwelling Incident Irradiance at a Footprint Located at  $R/2$** 

$k$	-1	0	1	2	3	4	5	6	7	8	9
$C_k$ $z = 0$ m	—	0.0555	0.3039	0.4972	0.5599	0.5321	0.4554	0.3544	0.2412	0.1219	0.0204
$C_k$ $z = -0.063$ m	0.0250	0.1732	0.4058	0.5050	0.5141	0.4712	0.3993	0.3107	0.2120	0.1074	0.0180

the same instrument. To within round-off error, the sum of the  $C_k$  coefficients is  $\pi$ .

These coefficients are valid when the ice surface is flush with the base of the dome ( $z = 0$ ). When the ice surface is depressed below the level of the dome base, the coefficients need to be recalculated. This was frequently the case, as the height of the ice surface was rarely predictable as the ice grew and sublimated. For an ice surface 6.3 cm below the dome floor, the  $C_k$  values are given in the second row of Table 1 ( $z = -0.063$  m). This positioning necessitates an additional measurement of radiance 10 deg below the base of the dome ( $k = -1$ ), which falls on the inside wall of the ice tank, as the radiance leaving the wall of the tank contributes to the total illumination on the ice surface. The sum of  $C_k$  ( $z = -0.063$  m) is also approximately  $\pi$ , as both integrations ( $z = 0$  and  $z = -0.063$  m) occur only over the transformed coordinate system  $\theta_f = 0$  to 90.

#### D. Estimation of Surface-Leaving Backscattered Irradiance at the Footprint

The total backscattered irradiance leaving the footprint was estimated by measuring the radiance field at the footprint location and integrating [as in Eq. (1)] to estimate the upwelling irradiance ( $F_f^\uparrow$ ). Radiance measurements were made using the same bare fiber optic probe as the dome-leaving radiances, but through the 60 and 34.4 deg viewing ports. Use of a bare fiber viewed through the ports eliminates shadows that would appear if a detector were physically placed inside the dome.

Since the incident radiance field was diffuse and the surface approximately Lambertian, we assumed the surface-leaving radiance distribution to be isotropic. Two measurements of the surface-leaving radiance were recorded, one at 0 deg zenith (looking straight down from the 60 deg port), and the other at 30 deg zenith (viewed from the 34.4 deg port). We initially attempted to collect radiance data also at 70 deg zenith angle (viewed through the 10.3 deg port), but that measurement proved to be unreliable since the finite acceptance cone of the bare fiber made it difficult to avoid contamination by incident light backscattered directly from the reflecting plate. This made integration by standard quadrature methods impossible. The integration of irradiance was carried out by assuming isotropy of the upwelling radiance field, and so the two radiances were simply averaged:

$$F_f^\uparrow = \pi \times \text{avg}(I_0, I_{30}).$$

$I_0$  and  $I_{30}$  were typically within 10% of each other at all wavelengths. Unlike the incident irradiance, integration of the backscattered irradiance is independent of the height of the ice surface relative to the dome floor.

#### 4. VALIDATION

A validation test for the albedo dome was carried out by comparing the field albedo of a white tarp surface measured

outdoors with the albedo dome technique applied to a sample of the same tarp cut to fit and laid on top of the ice surface in the laboratory ice tank. The two spectral albedos of the same material, measured using the two different techniques, were compared directly.

The albedo of a large (approximately 6 m  $\times$  9 m) white plastic tarp was measured outdoors in a flat parking lot (see Fig. 1). The field albedo measurements were made under uniform overcast sky with relatively steady illumination. Ten albedo measurements were made in succession and averaged to ensure that the effects of small variations in illumination or spectroradiometer leveling were minimized. The same spectroradiometer that was used in the laboratory measurements was used to measure the field albedo. For the field albedo measurements, the spectroradiometer was outfitted with a cosine collector for collecting upwelling and downwelling irradiances (as in Fig. 1). The white tarp itself was not opaque, so a sheet of optically thick black landscape plastic was laid down on the pavement first. This served to protect the white tarp from getting soiled, but the combination of plastic and tarp also served as an optically thick, reproducible surface. Figure 6 shows the spectral albedos of the tarp measured in the field using a cosine collector and in the laboratory using the albedo dome.

### 5. DISCUSSION

#### A. Albedo Comparison

The field albedo measurement is an established technique, so we treat it as “ground truth” for this comparison. Several tests, however, were applied to the field albedo to verify its accuracy. The effects of the finite size of the tarp were estimated by making albedo measurements at a variety of locations proximal to

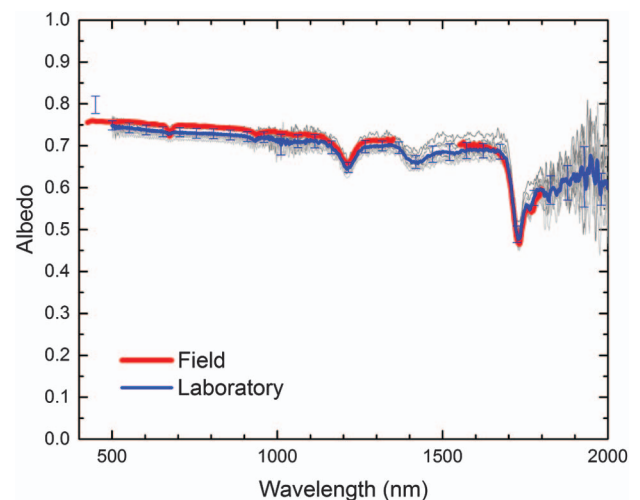


**Fig. 6.** Field and laboratory spectral albedo for white tarp test surface. Individual gray lines indicate the 10 individual laboratory albedo measurements made, and error bars indicate their standard deviation.

the center of the tarp, but offset from it. No variation was observed, so we conclude that no horizontal boundary effects were observed in the field albedo measurement. However, a shadowing correction was applied to the field albedo. Brandt *et al.* [27] estimated a correction for the shadows of the instrument and the operator using geometric analysis to be 1.7% for this particular setup for diffuse incidence. We applied this correction by multiplying the albedo at each wavelength by 1.017.

The field albedo could not be measured between 1350 and 1550 nm due to absorption of almost all natural insolation at these wavelengths by atmospheric water vapor. Likewise, light at wavelengths longer than 1800 nm is also strongly attenuated by the atmosphere, so albedos tend to be noisy at these wavelengths, as well. In contrast, the laboratory measurements have no spectral dropout, as the continuous output of the halogen bulb provides ample light at these wavelengths. However, wavelengths shorter than 500 nm and longer than 1800 nm do not produce reliable measurement in the laboratory, where reduced instrument sensitivity and lower bulb output combine to produce radiance estimates too noisy to be reliable. This limitation was largely caused by the extreme space constraints of our freezer laboratory. Headspace above the dome was limited to about 10 cm, so it was difficult to position a light source with higher output, which could have delivered significantly more light to the Spectralon plate. We anticipate that had there been more space, the removal of the mirror and replacement with a downwelling light source in its place would have produced adequate light for acceptable signal-to-noise ratio at wavelengths shorter than 500 nm, as well as longer than 1800 nm.

The variability of the albedo dome measurements is significantly larger than the variability of the field albedo measurements. The standard deviation of the laboratory measurements is indicated in Fig. 6 and is generally  $<2\%$  at wavelengths shorter than about 1000 nm and typically closer to 3.5% at longer wavelengths. For the field albedo, the observed variability was less than the line width on Fig. 6. The variability of the field albedo is tightly tied to the constancy of the incident illumination, and the incident light was notably steady over the time the 10 measurements were made (duration about 10 min near local solar noon). For the laboratory measurements, variability is tied to the repeatability of the radiance measurements for both incident and backscattered fields. Relative to the field albedo, the average of the laboratory measurements (blue curve in Fig. 6) is biased slightly low (about 2%) at all wavelengths shorter than about 1600 nm, but the agreement is generally favorable.

## B. Limitations and Uncertainties

The albedo dome technique is limited to estimation of the albedo under diffuse illumination conditions. It is ideally suited for estimating the spectral albedo of multiply scattering media with approximately isotropic backscattering. Surfaces with large specular reflectance or highly anisotropic BRDF would be difficult to characterize using this method, although estimation of a diffuse albedo should still be possible because the incident light is diffuse. Surfaces with high albedo generate a more uniform incident light field due to multiple reflections between surface and dome interior, likely reducing the measurement

error. The difference in albedo for diffuse illumination and direct illumination depends on the nature of the surface being measured. In the case of snow, the largest differences occur at wavelengths with moderate absorption (Fig. 11(a) of Wiscombe and Warren [28]). Wavelengths with little absorption display enough multiple scattering that the albedo does not depend on the relative fraction of direct-to-total radiation and it is generally very high, and wavelengths with large absorption display little scattering and the albedo is low, again making the character of the incident illumination of little importance. The albedo for a direct beam at the global-average solar zenith angle of  $60^\circ$  is approximately the same as the albedo for diffuse incidence.

Because the footprint size on the measurement surface is finite, it must be assumed to be representative of the entire surface. A surface that is not horizontally homogeneous is problematic beyond mere violation of the assumption of representativeness, as the radiance field reflected from the dome interior could have significant azimuthal variation if the surface were highly inhomogeneous. This would make the integration of downwelling irradiance from estimated radiances at a single longitude difficult. Another significant limitation of the albedo dome is the intensity of the source. Even with a 750 W tungsten-halogen bulb, most of the measured radiance fields were close to the limit of detection at some wavelengths, forcing us to rely heavily on the automatic accounting of variable dark level within the spectroradiometer. A single dark-level correction taken at the beginning of a set of albedo scans was applied to each scan. Precautions were taken to keep the instrument well insulated in the cold environment, but it is possible that dark levels did drift during individual experiments.

A number of potential biases inherent in the albedo-dome technique have been identified. Concerted effort was made to track down light leakage into the dome, specifically light that enters the entry port at directions that miss the reflecting plate on the ice surface. During the course of development, numerous bright spots on the dome interior were spotted, and efforts to baffle these spots were made. Any light entering the dome that causes a less azimuthally isotropic dome interior radiance field will bias the measurements.

An additional bias is due to the finite field of view of the bare fiber-optic cable. The numerical aperture of this fiber yields an acceptance cone of  $12.5^\circ$  half angle. The processing algorithm for integrating both downwelling and backscattered irradiances assumes that the measured radiances had zero angular divergence. Such idealized radiances are not practical to measure, but this assumption greatly simplified the processing. A bias results from the imprecision of these radiance estimates, where neighboring radiances essentially overlap. Perhaps the most problematic case is that of the measurement of backscattered radiance at  $30^\circ$ , where the large field of view likely included some of the ice that was partially shaded by the reflecting plate. This would impose a low bias on the albedo. Unfortunately, this is a difficult bias to quantify. Attempts to narrow the fiber's field of view were made with a collimating lens, but this reduced the signal recorded by the spectroradiometer.

Another bias results from the inability to accurately measure wall-leaving radiances at low elevation angles on the dome

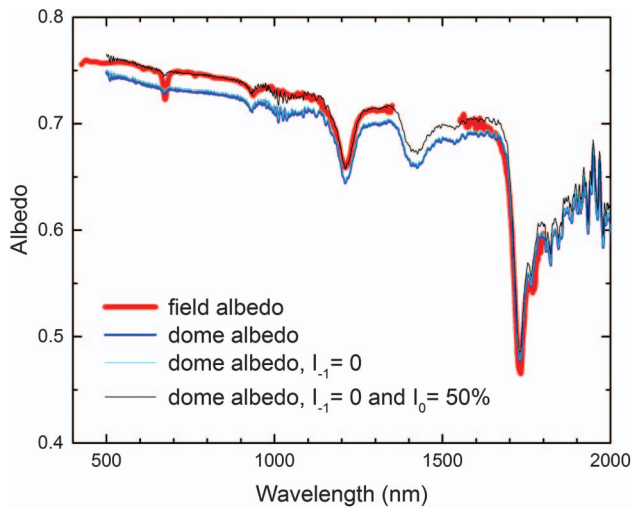


**Fig. 7.** Albedo sensitivities for quantifying the effects of overestimating the incident radiance profile at low dome latitudes.

interior. Measurements at  $k = 2, 1, 0$ , and  $-1$  were consistently contaminated with direct light from the reflecting plate. Linear extrapolation of radiances measured at higher elevation angles is probably reasonable for the angles that actually fall on the dome wall ( $k = 2, 1$ ). Extrapolation of these radiances that fall at the base of or below the dome wall ( $k = 0, -1$ ) should bias the albedo low, as it will consistently overestimate the incident irradiance owing to the relatively dark tank walls that were not measured. If the tank walls are brighter than the dome, then this would mean the incident irradiance is underestimated and the albedo is biased high, but this was generally not the case. The walls of the tank are gray plastic, and the top edge of the translucent plastic liner could also be seen in front of the tank wall. The reflectivity of this surface was not measured, but it is generally smaller than that of the highly reflecting dome interior. A sensitivity analysis was carried out to estimate a correction for the albedo-dome data due to this effect. Figure 7 shows the calculated albedo-dome result for the white tarp measurement with no contribution from the tank walls,  $I_{k=-1} = 0$  (cyan line), and for  $I_{k=-1} = 0$  and  $I_{k=0}$  reduced by 50% (green line). A 50% reduction of  $I_{k=0}$  would account for the fact that, at  $\theta = 0$ . Only half of the field of view sampled by the fiber

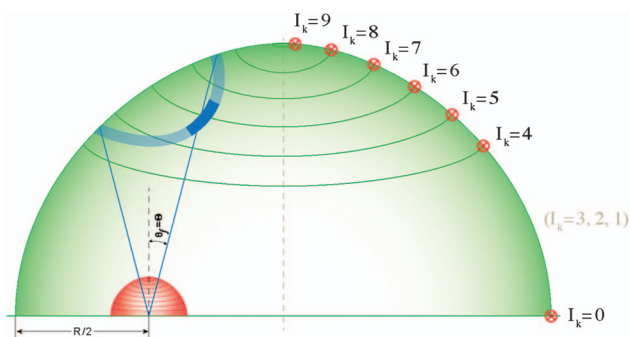


**Fig. 8.** Schematic drawing of the implementation of Eq. (A2). The blue band illustrates one term in the series, as detailed in Eq. (A3).

optic is occupied by the dome wall; the rest is the relatively dark tank wall. This adjustment caused the dome albedo to agree with the field albedo (Fig. 7). We have used this simple correction in the processing of incident irradiance for our studies of artificial sea ice and the development of the salt crust [29].

## 6. CONCLUSIONS

We have described a technique for estimating the spectral albedo of cold, laboratory-grown saline ice in a freezer laboratory. The development of this method was motivated by the need to measure the flux-reflectance (albedo) of a laboratory proxy for cold, sublimating sea ice not currently found in nature. The technique requires a simple list of equipment: hemispherical dome prepared with reflecting interior surface and light-blocking exterior surface, collimated broadband light source, mirror, Lambertian reflecting plate, and spectroradiometer with a fiber optic probe. This albedo-dome technique was validated by comparison of field and laboratory albedos applied to samples of a white tarp material. The validation experiment yielded agreement at wavelengths between 500 and 1800 nm that was generally within 2%.

We expect this technique to be applicable to a variety of surfaces that can be created in the laboratory. The principal requirement for a surface is horizontal homogeneity over the area beneath the dome. Materials with significant specular reflection or non-Lambertian BRDF can be used in the albedo dome to estimate diffuse albedo, but no information about the specular reflection or BRDF can be learned from this technique. Techniques that do measure the full BRDF provide a more comprehensive characterization of the surface, but this method has been implemented in a cold ( $T < -25^\circ\text{C}$ ) environment and uses only simple materials and a simple measurement protocol to describe the reflectance properties of media with long optical path lengths, such as snow and ice.

Both biases and random errors have been investigated for this technique. The most significant bias appears to stem from the inability to make direct dome-leaving radiance measurements at low latitudes on the dome. Having such measurements would increase the accuracy of the estimated incident irradiance. Without such measurements, we suspect the albedo is biased low. Additional bias may result from uncertainty of the backscattered radiance measurement at 30 deg, where it is possible that parts of the surface within the fiber optic field of view have been shadowed by the reflecting plate.

The most significant random errors appear to be a result of lack of repeatability in the measurements using the handheld fiber optic cable. Efforts were continually made to improve this repeatability, but clearly more improvement can be made. Additionally, there was concerted effort to track down light leakage into the dome from stray light emanating from the source. While baffles were constructed to eliminate this stray light, it is likely that not all leakage was prevented. Despite the bright appearance of the 750 W bulb, individual radiance measurements were often at the limit of detection for our spectroradiometer. The system would be improved with better beam collimation and other ways for increasing the intensity of light inside the dome. In this implementation, space constraints prevented alternative paths for the incident light that

would have yielded higher light intensities delivered to the interior reflecting plate. Development of a more portable version of this laboratory tool would also be advantageous, such that albedo dome measurements could be made in a larger variety of settings and locations.

## APPENDIX A

Following Eq. (1), the downwelling irradiance incident at the location of the footprint can be written as the integral

$$F_f^\downarrow = \int_0^{\pi/2} \int_0^{2\pi} I(\theta_f, \phi_f) d\phi_f \cos \theta_f \sin \theta_f d\theta_f, \quad (\text{A1})$$

where subscript  $f$  pertains to the virtual hemisphere centered on the footprint (red dome in Fig. 5). The integral of radiance for a particular  $\theta_f$  over all azimuth angles  $\phi_f$  can be expressed as a weighted series calculated from the dome-leaving radiances  $I_k$  measured on the dome interior:

$$\int_0^{2\pi} I(\theta_f, \phi_f) d\phi_f = \sum_k m_k(\theta_f) I_k, \quad (\text{A2})$$

where the  $m_k$  are weightings. Subscript  $k$  indicates the discrete locations where surface-leaving radiance is measured on the albedo dome. In our treatment,  $k$  varies from  $-1$  to  $9$ , but more measurements could be made and  $k$  could have a larger range. Figure 8 illustrates the integration of Eq. (A2) for one such blue band. In this purely illustrative example,

$$\begin{aligned} \int_0^{2\pi} I(\theta_f = \Theta) d\phi_f &= \sum_k m_k(\Theta) I_k \\ &= 2 \cdot m_5 I_5 + 2 \cdot m_6 I_6 + 2 \cdot m_7 I_7, \end{aligned} \quad (\text{A3})$$

where the  $m_k$  correspond to the length of the arc in radians that passes through each  $k$  band. The  $m_6 I_6$  term is indicated by the darker portion of the blue band in Fig. 8. The sum of all  $m_k$  must equal  $2\pi$ .

The list of  $I_k$  values included for each  $\theta_f$  is known from a list of dome intersect points that maps each  $(\theta_f, \phi_f)$  pair with its corresponding  $(\theta, \phi)$  pair on the albedo dome. This relationship is compiled by taking a unit vector through each  $(\theta_f, \phi_f)$  pair and calculating the  $(\theta, \phi)$  pair where it intersects with the outer dome.

Substituting Eq. (A2) into Eq. (A1),

$$F_f^\downarrow = \int_0^{\pi/2} \frac{1}{2} \sin(2\theta_f) \left[ \sum_k m_k(\theta_f) I_k \right] d\theta_f, \quad (\text{A4})$$

and rewriting as a sum,

$$F_f^\downarrow = \sum_0^{\pi/2} \frac{1}{2} \sin(2\theta_f) \left[ \sum_k m_k(\theta_f) I_k \right] \Delta\theta_f, \quad (\text{A5})$$

we can then assign

$$C_k = \sum_0^{\pi/2} \frac{1}{2} \sin(2\theta_f) \Delta\theta_f m_k(\theta_f) \quad (\text{A6})$$

such that

$$F_f^\downarrow = \sum_k C_k I_k, \quad (\text{A7})$$

which is Eq. (2) in the main text.

United States National Science Foundation Office of Polar Programs (OPP) (ANT-0739779, ANT-1142963).

The capable laboratory assistance of Ruzica Dadic, Alan Wright, and Taryn Black is gratefully acknowledged. Thanks also to Matt Wyant for sage technical advice and production of Figure 5, and to Richard E. Brandt for fruitful discussion and loan of the Oriel collimator. An anonymous reviewer provided helpful comments.

## REFERENCES

1. W. S. Pegau and C. A. Paulson, "The albedo of Arctic leads in summer," *Ann. Glaciol.* **33**, 221–224 (2001).
2. D. K. Perovich, T. C. Grenfell, B. Light, and P. V. Hobbs, "Seasonal evolution of the albedo of multiyear Arctic sea ice," *J. Geophys. Res.* **107**, 1–13 (2002).
3. L. D. D. Harvey, "On the role of high latitude ice, snow, and vegetation feedbacks in the climatic response to external forcing changes," *Clim. Change* **13**, 191–224 (1988).
4. C. Covey, K. E. Taylor, and R. E. Dickinson, "Upper limit for sea ice albedo feedback contribution to global warming," *J. Geophys. Res.* **96**, 9169–9174 (1991).
5. J. E. Walsh, "Intensified warming of the Arctic: causes and impacts on middle latitudes," *Glob. Planet. Change* **117**, 52–63 (2014).
6. R. G. Graversen, P. L. Langen, and T. Mauritsen, "Polar amplification in CCSM4: contributions from the lapse rate and surface albedo feedbacks," *J. Clim.* **27**, 4433–4450 (2014).
7. J. E. Kay, M. M. Holland, C. M. Bitz, E. Blanchard-Wrigglesworth, A. Gettelman, A. Conley, and D. Bailey, "The influence of local feedbacks and northward heat transport on the equilibrium arctic climate response to increased greenhouse gas forcing," *J. Clim.* **25**, 5433–5450 (2012).
8. M. C. Serreze and R. G. Barry, "Processes and impacts of Arctic amplification: a research synthesis," *Glob. Planet. Change* **77**, 85–96 (2011).
9. R. Levinson, H. Akbari, and P. Berdahl, "Measuring solar reflectance—part II: review of practical methods," *Sol. Energy* **84**, 1745–1759 (2010).
10. T. C. Grenfell, S. G. Warren, and P. C. Mullen, "Reflection of solar radiation by the Antarctic snow surface at ultraviolet, visible, and near-infrared wavelengths," *J. Geophys. Res.* **99**, 18669–18684 (1994).
11. D. K. Perovich and T. C. Grenfell, "Laboratory studies of the optical properties of young sea ice," *J. Glaciol.* **27**, 331–346 (1981).
12. O. L. Hadley and T. W. Kirchstetter, "Black-carbon reduction of snow albedo," *Nat. Climate Change* **2**, 437–440 (2012).
13. H. W. O'Brien and R. H. Munis, "Red and near-infrared spectral reflectance of snow," CRREL Res. Rep. 332 (U. S. Army Cold Regions Research and Engineering Laboratory, Hanover, N.H., 1975), Available as NTIS AD-A007 732/IGI, from the National Technical Information Service, Springfield, Va.
14. B. Barkey and K. N. Liou, "Laboratory measurements of spectral reflection from ice clouds of various habits," *Appl. Opt.* **45**, 5716–5724 (2006).
15. B. Barkey and K. N. Liou, "Visible and near infrared reflectances measured from laboratory ice clouds," *Appl. Opt.* **47**, 2533–2540 (2008).
16. O. Brissaud, B. Schmitt, N. Bonnefoy, S. Douté, P. Rabou, W. Grundy, and M. Fily, "Spectrogonio radiometer for the study of the bidirectional reflectance and polarization functions of planetary surfaces. 1. Design and tests," *Appl. Opt.* **43**, 1926–1937 (2004).
17. S. Sandmeier, C. Muller, B. Hosgood, and G. Andreoli, "Sensitivity analysis and quality assessment of laboratory data," *Remote Sens. Environ.* **64**, 176–191 (1998).

18. C. A. Coburn and D. R. Peddle, "A low-cost field and laboratory goniometer system for estimating hyperspectral bidirectional reflectance," *Can. J. Remote Sens.* **32**, 244–253 (2006).
19. D. Biliouris, W. W. Verstraeten, P. Dutré, J. A. N. van Aardt, B. Muys, and P. Coppin, "A compact laboratory spectro-goniometer (CLabSpeG) to assess the BRDF of materials. Presentation, calibration and implementation on *Fagus sylvatica* L. leaves," *Sensors* **7**, 1846–1870 (2007).
20. G. T. Georgiev, C. K. Gatebe, J. J. Butler, and M. D. King, "BRDF analysis of savanna vegetation and salt-pan samples," *IEEE Trans. Geosci. Remote Sens.* **47**, 2546–2556 (2009).
21. P. F. Hoffman and D. P. Schrag, "The snowball Earth hypothesis: testing the limits of global change," *Terra Nova* **14**, 129–155 (2002).
22. S. G. Warren, R. E. Brandt, T. C. Grenfell, and C. P. McKay, "Snowball Earth: Ice thickness on the tropical ocean," *J. Geophys. Res.* **107**, 31-1–31-18 (2002).
23. C. P. McKay, "Thickness of tropical ice and photosynthesis on a snowball Earth," *Geophys. Res. Lett.* **27**, 2153–2156 (2000).
24. W. F. Weeks and S. F. Ackley, "The growth, structure, and properties of sea ice," in *The Geophysics of Sea Ice*, N. Untersteiner, ed. (Plenum, 1986), pp. 9–164.
25. R. Carns, R. E. Brandt, and S. G. Warren, "Salt precipitation in sea ice and its effect on albedo, with application to Snowball Earth" (manuscript in preparation).
26. E. M. Patterson, C. E. Shelden, and B. H. Stockton, "Kubelka-Munk optical properties of a barium sulfate white reflectance standard," *Appl. Opt.* **16**, 729–732 (1977).
27. R. E. Brandt, S. G. Warren, and A. D. Clarke, "A controlled snow-making experiment testing the relation between black carbon content and reduction of snow albedo," *J. Geophys. Res.* **116**, D08109 (2011).
28. W. J. Wiscombe and S. G. Warren, "A model for the spectral albedo of snow. I: pure snow," *J. Atmos. Sci.* **37**, 2712–2733 (1980).
29. B. Light, R. Carns, and S. G. Warren, "Laboratory measurements of the spectral albedo of surrogate ocean surfaces on Snowball Earth: I. observations" (manuscript in preparation).